Amelioration of white matter injury through mitigating ferroptosis following hepcidin treatment after spinal cord injury

Shengli Hu (husl1937@163.com)
Third Military Medical University: Army Medical University https://orcid.org/0000-0001-6438-6924
Jiantao Shi
Third Military Medical University Southwest Hospital
Xingshen Xue
Third Military Medical University: Army Medical University
Linbo Yuan
Third Military Medical University Southwest Hospital
Guangjian He
Third Military Medical University Southwest Hospital
Zhouyang Jiang
Third Military Medical University Southwest Hospital
Long Wang
Third Military Medical University Southwest Hospital
Jiali Zhang
Third Military Medical University Southwest Hospital
Hong su
Third Military Medical University Southwest Hospital
Jishu Xian
Third Military Medical University Southwest Hospital
Chuhua Fu
Hubei University of Medicine

Research Article

Keywords: spinal cord injury, hepcidin, ferroptosis, white matter injury, reactive oxygen species

Posted Date: November 2nd, 2022

DOI: https://doi.org/10.21203/rs.3.rs-2210591/v1

Version of Record: A version of this preprint was published at Molecular Neurobiology on February 28th, 2023. See the published version at https://doi.org/10.1007/s12035-023-03287-x.

Abstract

Spinal cord injury (SCI) usually introduces permanent or long-lasting neurological impairments. Maintaining the integrity of limited number of white matter bundles (5–10%) preserves wholly or partially locomotor following SCI. Considering that the basic structure of white matter bundles is axon wrapped by oligodendrocytes, promoting oligodendrocytes survival might be a feasible strategy for reducing white matter injury (WMI) after SCI. Oligodendrocytes are rich in unsaturated fatty acid, and susceptible to ferroptosis-induced damage. Hence, exploring method to reduce ferroptosis is supposed to expedite oligodendrocytes survival, thereafter mitigating WMI to facilitate functional recovery post-SCI. Here, the results indicated the administration of hepcidin reduced iron accumulation to promote oligodendrocytes survival and to decrease spinal cord atrophy, thereafter facilitating functional recovery. Then, the WMI was evidently decreased due to attenuating ferroptosis. Subsequently, the results uncovered that the expression of divalent metal transporter 1 (DMT1) and transferrin receptor 1 (TfR1) was expressed in $CC1^+$ cells. The expression level of DMT1 and TfR1 was significantly increased, while this phenomenon was obviously neutralized with the administration of hepcidin in the epicenter of spinal cord after SCI. Afterward, the application of hepcidin downregulated reactive oxygen species (ROS) overload, which was evidently increased with the treatment of 20 μM $FeCl_3$, thereafter increasing cell viability and reducing lactate dehydrogenase (LDH) activity through downregulating the expression of DMT1 and TfR1 to inhibit ferroptosis in oligodendrocyte progenitor cells (OPCs). The present study provides evidence that the application of hepcidin expedites oligodendrocytes survival to alleviate WMI via minimizing the expression of DMT1 and TfR1.

1. Introduction

Spinal cord injury (SCI), a devastating injury with serious consequences and a small chance of recovery, usually introduces permanent or long-lasting neurological impairments [1, 2]. The pathology of neurological deficits ascribes to primary and secondary injury. The effective therapy for primary injury is surgery, while the mechanism of secondary injury is complicated. Therefore, targeting secondary injury is a feasible regimen for mitigating neurological deficits after SCI. Our previous studies have found out a series of therapeutic candidates targeting secondary damage, including reducing glial scar formation and enhancing axon rehabilitation through the administration of curcumin, antisense vimentin cDNA combined with chondroitinase ABC [3–5], decreasing neuronal loss by blocking acid-sensing ion channel 1a (ASIC 1a) [6] or activating G-protein coupled estrogen receptor 1 (GPER1) [7, 8], and suppressing complement C5a [9]. Cell replacement therapy including promoting endogenous neural stem cell (NSC) differentiation into neurons [10, 11] and the transplantation of human umbilical cord mesenchymal stem cell (MSC) [12] shows some beneficial performance in SCI model. However, the therapeutic effect is still far from ideal, suggesting that more mechanisms related to secondary injury need to be elucidated.

Our previous studies have mainly focused on the research of neuronal damage, survival and regeneration of neurons. However, recent studies have indicated that maintaining the integrity of limited number of white matter bundles (5–10%) could preserve wholly or partially locomotor during the acute and/or

chronic stage of SCI [13–15]. Given that the basic structure of white matter bundles is axon wrapped by oligodendrocytes, promoting oligodendrocytes survival might be a feasible strategy for preserving the integrity of white matter bundles to reduce white matter injury (WMI) after SCI. Oligodendrocytes, the main neural subtype responsible for surrounding axons in the central nervous system (CNS), are rich in unsaturated fatty acid [4] and susceptible to ferroptosis-induced damage [16]. Ferroptosis, a form of nonapoptotic form of cell death, is characterized by iron-dependent lipid peroxidation, and ferroptotic cells exhibit shrunken mitochondria, smaller mitochondrial area and increased membrane density [17, 18]. Previous studies have demonstrated ferroptosis is a common pathology resulting from iron and reactive oxygen species (ROS) overload in the epicenter of spinal cord following SCI [17, 19, 20]. Herein, exploring method to reduce ferroptosis is supposed to expedite oligodendrocytes survival, thereafter mitigating WMI to facilitate functional recovery post-SCI.

Hepcidin is a secreted peptide hormone encoded by the hepcidin antimicrobial peptide (HAMP) gene and generated mainly by the liver [21]. Increased hepcidin expression decreases iron content by binding with ferroportin 1 (Fpn1) and then blocks iron export from hepatocytes, enterocytes, cardiomyocytes, and macrophages [21–23]. The administration of hepcidin peptide evidently downregulates the expression of cell-iron-uptake proteins including transferrin receptor 1 (TfR1) and divalent metal transporter 1 (DMT1), thereafter reducing iron release in cultured microvascular endothelial cells [24]. Furthermore, hepcidin holds the capacity of reducing iron uptake and release in cultured astrocytes and neurons through decreasing the expression of Fpn1, TfR1 and DMT1 [24, 25], suggesting that the application of hepcidin might downregulate TfR1 and DMT1 to alleviate oligodendrocytes injury after SCI. However, the effect of hepcidin on reducing WMI and the underlying mechanism remains elusive.

In the present study, we posited that oligodendrocytes ferroptosis induced by iron and ROS overload played an important role in WMI after SCI, and the application of hepcidin might mitigate oligodendrocytes ferroptosis via reducing iron and ROS accumulation through downregulating the expression of TfR1 and DMT1, thereafter inhibiting WMI to promote functional recovery post-SCI. The aim of the present study is to certify the therapeutic effects of hepcidin on SCI in rats, and to offer a possible therapeutic strategy for SCI, even for other CNS diseases existing ferroptosis, from bench to bedside.

2. Materials And Methods

2.1. Animals

The animal experiment procedures were implemented according to the China's animal welfare legislation for the protection of animals used for scientific purposes, and supervised by the Ethics Committee of the Southwest Hospital, Third Military Medical University (Army Medical University) for the use of laboratory animals (approval no. AMUWEC20210017). A total of 20 P0–P1 Wistar rats and 78 adult female (200–250 g, 10–12 weeks, 118 rats used for experiments and 8 rats died during experiments) Wistar rats were used for establishing spinal cord injury (SCI) in the present study. All rats were housed in a constant

condition (12-h light/dark cycle, 22–25°C, 55–60% moisture) and given free access to food and water before and after surgery.

2.2. The establishment of rat spinal cord injury (SCI) model

The rat SCI model was established as previously described [1, 26]. Briefly, a stereotaxic frame was applied to fixed the rats after they were anaesthetized with 2% isoflurane/air mixture (2–3 l/min). Then, a 4-cm-long skin incision was made in the midline of the back over the spinal cord, and the thoracic 9–11 (T9-11) spinal segments was exposed by performing a laminectomy, leaving the dura intact. Afterward, spinal contusion was implemented using a 20-g weight rod (diameter 4 mm) dropping from a height of 30 mm onto the exposed T10 segment. Subsequently, the muscles, subcutaneous tissue and skin were separately sutured. During surgery, rat body temperature was maintained at 37 ± 0.3°C using a feedback-controlled heating pad system (Zhongshi, inc., Beijing, China). After surgery, rats were received manual bladder empty twice a day until they could do themselves. The dehydration, weight loss, autophagia and discomfort were recorded per day, even with appropriate veterinary care if needed.

2.3. Experimental groups

After surgery, rats were randomly divided into the following groups using the random number table method:

1. Sham group. Rats, received laminectomy without contusion, were intra-spinally microinjected the same volume of 0.01 M phosphate buffered saline (PBS, pH 7.4), equivalently to the volume of hepcidin solution in SCI + hepcidin group, using the same method.
2. SCI group. Rats, received laminectomy with contusion, were intra-spinally microinjected the same volume 0.01 M PBS (pH 7.4), equivalently to the volume of hepcidin solution in SCI + hepcidin group, using the same method.
3. SCI + hepcidin group. Rats, received laminectomy with contusion, were intra-spinally microinjected recombinant mouse hepcidin (cat no. RPB979Mu01, 0.7 mg/kg, Cloud-Clone Corp., Katy, TX, USA) four hours after surgery. Hepcidin was diluted in 0.01 M PBS (pH 7.4), and microinjected into the dorsal spinal cord 2 mm rostrally and 2 mm caudally to the injury site at a depth of 1.2 mm and 0.75 mm laterally from midline at a rate of 1 μl/min. Afterward, the needle was left in position for a further 2 min before being slowly withdrawn. A total volume of 10 μl hepcidin was injected. The second dosage was performed on the second day after SCI.

2.4. The Basso, Beattie, and Bresnahan (BBB) locomotor rating score

The BBB locomotor rating score is a 21-point scale that is universally applied to determine the behavioral outcomes after SCI in rats [27]. The rating score ranges from 0 to 21: 0 exhibits no locomotor function and 21 shows normal performance. In short, rats were placed in a 90-cm^2 field and allowed them to walk around freely for 5 min, and the movements of hind limb were closely observed and recorded using a

camera. Subsequently, the BBB locomotor rating score was assessed by two independent examiners blinded to the experimental groups on days 7, 35 and 56.

2.5. Primary oligodendrocyte progenitor cells (OPCs) culture

Primary OPCs were isolated from P0–P1 Wistar rats as previously described [1]. In brief, the spinal cord tissues were dissected under a stereomicroscope (SZ61, Olympus, Tokyo, Japan) after the dura mater and blood vessels were removed. Thereafter, the samples were triturated using a fire-polished Pasteur pipette and the cell suspensions were passed through a 40-μm Nylon cell strainer (Nest, Wuxi, China). Afterward, the cell suspensions were cultured in Dulbecco's modified Eagle's medium (DMEM; Hyclone, Logan, Utah, USA) supplemented with 20% fetal calf serum after centrifugation at 1000 rpm. The culture medium was replaced every 2–3 days.

After 10–12 days, immature oligodendrocytes were collected by shaking overnight at 230 rpm. Then, the cell suspensions were pre-seeded for 30 min at 37°C under 5% CO_2 to remove contaminating astrocytes and microglia. Afterward, floating cells were plated on poly-L-ornithine-coated (Sigma-Aldrich, Munich, Germany) cover slips or culture plates (1×10^5 cells/ml) and cultured in DMEM supplemented with 2% B27 (Gibco, Grand Island, NY, USA), 10 ng/ml basic fibroblast growth factor (bFGF, Peprotech, Rocky Hill, NJ, USA) and 10 ng/ml plated derived growth factor (PDGF, Peprotech, Rocky Hill, NJ, USA). Thereafter, the purity of cells was determined by co-labelling of NG2 and PDGFαR using immunostaining.

Hepcidin was firstly dissolved in 0.01 M PBS (pH 7.4) and then diluted with culture medium with the final concentration of 0.5 μM for *in vitro* experiments. The control or vehicle group was added the same volume of 0.01 M PBS (pH 7.4) as the hepcidin group.

2.6. Hematoxylin and Eosin (HE) staining

HE staining was performed to assess the injury and necrosis status of spinal cord after SCI [28]. Briefly, spinal cord sections were sliced using a freezing microtome, washed with distilled water, incubated in hematoxylin staining solution for 10 min, then rinsed with distilled water 3 times, differentiated in 0.1% hydrochloric acid-ethanol for 25 sec, blued in 0.01M PBS for 45 min followed by 95% alcohol washing for 5 sec, thereafter immersed in eosin staining solution for 1 min, dehydrated with 95% alcohol, cleared with xylene, and finally mounted on glass slides. Images were captured using a light microscope (Carl Zeiss, Weimar, Germany), and analyzed by individual investigators blinded to group assignment using an Image J software (ImageJ 1.8, NIH, USA).

2.7. Perl's blue staining

Perl's blue staining was applied to exhibit iron deposition as previously described [1]. The T10 spinal cord segments containing the injured epicenter and surrounding uninjured tissues (6 mm = 3 mm either side from the injury epicenter) were collected for preparing paraffin sections according to the standard procedures. Paraffin sections (5 μm) were deal with a graded ethanol series, immersed in xylene, and

rehydrated in PBS. Afterward, specimens were incubated in Perls' staining solution (comprising equal parts of potassium ferrocyanide and HCL) for 20 min. Subsequently, the samples were rinsed with Milli-Q water and stained cell nuclei with Fast Red solution for 5–10 min, dehydrated, cleared in xylem and mounted on glass slides. Images were photographed by a light microscope (Carl Zeiss, Weimar, Germany), and analyzed by individual investigators blinded to group assignment using an Image J software (ImageJ 1.8, NIH, USA).

2.8. Reactive oxygen species (ROS) measurement

ROS levels were measured by a ROS assay kit in accordance with the manufacturer's instruction (cat. no. S0033S, Beyotime, Shanghai, China). Primary OPCs were collected and homogenized on ice. Then, each sample was loaded with 500 μl 10 μM DCFH-DA and incubated in the dark at 37°C for 20 min. Afterward, the loading buffer was replaced and washed to eliminate residual DCFH-DA. Subsequently, the samples were immediately measured using a flow cytometer (ACEA Biosciences Inc., San Diego, CA, USA) with an argon laser (488 nm).

2.9. Immunohistochemistry (IHC)

For immunostaining, sections were incubated in 4% paraformaldehyde for 30 min at room temperature and permeabilized with 0.3% Triton-X 100 (Sigma-Aldrich, St. Louis, MO) in PBS. Then, samples were incubated in the following primary antibodies overnight at 4°C after being blocked with 5% bovine serum album (BSA, Sigma-Aldrich, St. Louis, MO), anti-CC1 (cat. no. OP44, Sigma-Aldrich, Munich, Germany), anti-DMT1 (cat. no. PA5-35136, Thermo Fisher Scientific, Waltham, MA, USA), anti-TfR1 (cat. no. PA5-116065, Thermo Fisher Scientific, Waltham, MA, USA), anti-NG2 (cat. no. MAB5384-I, Sigma-Aldrich, Munich, Germany), and anti-PDGFαR (cat. no. ab32570, Abcam, Cambridge, UK). On the second day, the samples were immersed in Alexa Fluor® 555 or 488-conjugated secondary antibody (1:100; cat. nos. A0453 and A0423; Beyotime Institute of Biotechnology, Beijing, China) for 2 hours at room temperature. The cell nuclei were counterstained with 4'-6-diamidino-2-phenylindole (DAPI; Beyotime, Shanghai, China) for 10 min at room temperature. Thereafter, the specimens were mounted onto glass slides, and images were captured using a confocal microscope (Carl Zeiss, LSM780, Weimar, Germany) and examined by individual investigators blinded to group assignment using a Zen 2011 software (Carl Zeiss, Weimar, Germany).

For immunohistochemistry, slices were dewaxed and antigen-repaired according to the standard procedures [29]. Then, samples were immersed in endogenous peroxidase for 10 min. Afterward, the specimens were immersed in anti-CC-1 (cat. no. SAB4501438, Sigma-Aldrich, Munich, Germany) primary antibody overnight at 4°C after being blocked with 5% BSA dissolved in 0.3% Triton-X 100 (Sigma-Aldrich, St. Louis, MO). After being washed, they were incubated in horseradish peroxidase (HRP)-conjugated goat anti-rabbit immunoglobulin G (ZSGB-BIO, Beijing, China). Then, the 3-diaminobenzidine (DAB) kit was employed to show the positive cells in brown color. Afterward, the sections were stained with hematoxylin and dehydrated with ethanol and xylene to mount onto glass slides. Images were photographed by a light microscope (Carl Zeiss, Weimar, Germany), and analyzed by individual investigators blinded to group

assignment using an Image J software (ImageJ 1.8, NIH, USA). For each sample, six sections were stained, analyzed, calculated and reported as the average of four independent measurements.

2.10. Transmission electron microscopy (TEM)

TEM was performed to visualized ultrastructural of myelin sheath and mitochondria status in each group, as previously described [1]. In brief, the samples containing the injured epicenter and surrounding uninjured tissues (2 mm = 1 mm either side from the epicenter) were firstly fixed in 1.25% glutaraldehyde overnight after perfusion. Then, the samples were post-fixed in 1.25% glutaraldehyde 3 days at 4℃. Thereafter, the specimens were washed and incubated in 1% citric acid (OsO4) for 2 h. Afterward, uranyl acetate was used for redyeing, and gradient acetone was used for dehydration. Then, an ultramicrotome (EM UC7, Leica, IL, USA) was used for slicing before the samples were infiltrated with propylene oxide, and embedded by epoxy. Images were photographed using a transmission electron microscope (Hitachi HT7700, Tokyo, Japan). At least three independent samples per group were analyzed by individual investigators blinded to group assignment using an Image J software (ImageJ 1.8, NIH, USA) to exhibit the myelin sheath thickness.

2.11. Western blot

The T10 spinal cord segments containing the injured epicenter and surrounding uninjured tissues (0.5 cm = 0.25 cm either side from the epicenter) were immediately collected after decapitation on day 7 post-SCI. The tissues were collected after being homogenized and the protein content of each sample was measured by a bicinchoninic acid (BCA) method (Beyotime, Shanghai, China). A total of 50 μg proteins were separated by 8 or 10% SDS-PAGE under reducing conditions and electro-blotted to polyvinylidene difluoride (PVDF, Roche, Indianapolia, IN, USA) membranes. Then, the membranes were blocked with 5% non-fat dry milk (Beyotime, Shanghai, China) in tris buffered saline (TBS) with Tween-20 (TBST) for 2 h at room temperature. Afterward, the samples were submerged in primary antibodies, anti-dMBP (cat. no. MBS618031, MybioSource, San Diego, CA, USA), anti-DMT1 (cat. no. PA5-35136, Thermo Fisher Scientific, Waltham, MA, USA), anti-APP antibody (cat. no. MAB348, Sigma-Aldrich, Munich, Germany), anti-TfR1 (cat. no. MA5-32500, Thermo Fisher Scientific, Waltham, MA, USA), or anti-GAPDH (cat. no. AF0006; Beyotime, Shanghai, China) overnight at 4°C. On the next day, the membrane was submerged in corresponding horseradish peroxidase (HRP)-conjugated secondary antibodies after being washed with TBST. All membranes were visualized by a ChemiDoc™ XRS$^+$ imaging system (Bio-Rad, California, USA) using the WesternBright ECL Kits (Beyotime, Shanghai, China). Densitometric density of each membrane was determined using an Image Lab™ software (Bio-Rad, California, USA), and analyzed by individual investigators blinded to group assignment.

2.12. Reverse transcription-quantitative polymerase chain reaction (RT-qPCR)

Total RNA was extracted using a TaKaRa MiniBEST Universal RNA Extraction Kit (cat no. 9767, TaKaRa, Tokyo, Japan) in accordance with the manufacturer's instructions after primary OPCs were gathered from each group. Then, a total of 1 μg RNA was reversely transcribed into cDNA using a PrimeScript RT

reagent Kit with gDNA Eraser (cat. no. RR0047A, TaKaRa, Tokyo, Japan). Subsequently, qPCR was performed using the CFX96 System (Bio-Rad, CA, USA) with SYBR Premix Ex TaqII (Tli RNaseH Plus) (cat. no. RR820A, TaKaRa, Tokyo, Japan) under the following condition: 95°C for 30 sec, 40 cycles at 95°C for 5 sec and 60°C for 30 sec. Relative mRNA levels were normalized to GAPDH and analyzed using the $2^{-\Delta\Delta Cq}$ method. Primer sequences used in the present study were listed in Table 1.

Table 1
Primer sequences for RT-qPCR.

Target genes	Forward primer sequence (5′-3′)	Reverse primer sequence (5′-3′)
DMT1	TGATCCTGACCCGGTCTATC	CAATCCTCCAGCCTATTCCA-
TfR	CTAGTATCTTGAGGTGGGAGGAAGAG	GAGAATCCCAGTGAGGGTCAGA
GAPDH	GACAACTTTGGCATTGTGG	ATGCAGGGATGATGTTCTG

2.13. Lactate dehydrogenase (LDH) releasing analysis

Lactate dehydrogenase (LDH) releasing level was evaluated using a LDH assay kit (Nanjing Jiancheng bioengineering inc., Nanjing, China) according to the manufacturer's instructions to assess cytotoxicity. Briefly, the respective supernatants were firstly collected, then neurospheres were lysed with 2% Triton X-100 for 15 min on ice to release all LDH from the cytoplasm. LDH released from cell lysates was measured to be the maximal LDH release and was used as positive controls. LDH releasing level was detected by a microplate reader (Thermo Fisher Scientific, Waltham, MA, USA) at the wavelength of 450 nm, and data were presented as the content of LDH (U/L) released in the medium.

2.14. Cell viability assay

The cell viability was determined by a cell counting kit-8 (CCK8; Dojindo, Tokyo, Japan), which uses a water-soluble tetrazolium salt to quantify the number of live cells by producing an orange formazan dye upon bio-reduction in the presence of an electron carrier. Briefly, 100 μl of cell suspension (1×10^5 cells/well) was dispensed in a 96-well cell culture cluster, then incubated in 10% (v/v) CCK8 solution for at 37°C 2.5 h. Then, the absorbance of the culture medium at a test wavelength of 450 nm was determined using a microplate reader (Thermo Fisher Scientific, Waltham, MA, USA) and a reference wavelength of 630 nm as well.

2.15. Statistical analysis

All data were expressed as mean ± SEM. The statistical analyses were implemented using SPSS 18.0 software (SPSS, Inc., Chicago, IL, USA). For statistical data collected at repeating time points were analyzed using two-way analysis of variance (ANOVA), followed by Turkey's post hoc test. For data with a single time point, multiple comparisons were performed by one-way ANOVA, followed by Turkey's post hoc test in case of the data with a normal distribution using a Shapiro–Wilk normality test. A $p < 0.05$ was considered to be statistical difference.

3. Results

3.1. Hepcidin improved functional recovery through decreasing iron accumulation and promoting oligodendrocytes survival in rats after SCI.

To assess the role of hepcidin in functional recovery after SCI, the BBB score was firstly performed. The results demonstrated that the BBB score of rats in SCI + hepcidin group was significantly higher than that in SCI group from day 7 to 56 (Fig. 1A). Then, the HE staining images showed that the administration of hepcidin obviously decreased the spinal cord atrophy that was apparently observed in the epicenter of injured spinal cords on day 7 post-SCI (Fig. 1B). And, the application of hepcidin evidently decreased the iron content using Perl's blue staining, whose level was clearly increased in the epicenter of injured spinal cord following SCI (Fig. 1C). Furthermore, the immunohistochemistry images depicted the number of $CC1^+$ cells were greatly decreased after SCI, while the administration of hepcidin obviously abrogated this effect (Fig. 5D, E). Collectively, these results illustrated that hepcidin facilitated functional recovery by reducing iron deposition and facilitating oligodendrocytes survival after SCI.

3.2. Hepcidin decreased WMI through mitigating ferroptosis on day 7 after SCI in rats.

Previous results had indicated that hepcidin promoted oligodendrocytes following SCI, the myelin sheath thickness was determined using TEM. The images demonstrated that the myelin sheath thickness was significantly decreased after SCI, while the application of hepcidin obviously increased the myelin sheath thickness (Fig. 2A, B). Meanwhile, the immunoblot blot bands presented that the expression of degraded myelin basic protein (dMBP) and amyloid precursor protein (APP) was predominantly increased after SCI, whereas this effect was substantially abolished with the treatment of hepcidin (Fig. 2C-E). Considering that iron accumulation always results in ROS production to induce ferroptosis [21], the status of ferroptosis was evaluated by TEM assays in each group. The TEM images illustrated that the proportion of shrunken mitochondria was surely elevated after SCI, while the application of hepcidin profoundly declined the percentage of depauperated mitochondria (Fig. 2F, G). Taken together, these results demonstrated that SCI triggered WMI via ferroptosis, and this phenomenon was partially compromised with the treatment of hepcidin.

3.3. Hepcidin compromised ferroptosis by downregulating the expression of DMT1 and TfR1 post-SCI.

Previous studies have demonstrated that cultured astrocytes and neurons expressed TfR1 and DMT1 [24, 25], while the expression of TfR1 and DMT1 was not elucidated. Here, the expression of TfR1 and DMT1 was determined using immunostaining. The representative images illustrated that DMT1 and TfR1 expressed in $CC1^+$ cells (Fig. 3A, B). Thereafter, the immunoblot bands demonstrated that the expression of DMT1 and TfR1 was gradually increased, and reached the peak on day 7 post-SCI (Fig. 3C-E). And, the

expression of DMT1 and TfR1 was still stayed at high level at least on day 56 (Fig. 3C-E). In addition, the administration of hepcidin significantly reduced the expression of DMT1 and TfR1, which was remarkably increased after SCI, on day 7 (Fig. 3F-H). Taken together, these results showcased that TfR1 and DMT1 expressed in oligodendrocytes and hepcidin reduced ferroptosis through decreasing the expression of DMT1 and TfR1 after SCI on day 7.

3.4. Hepcidin decreased ROS deposition to increase cell viability and reduce LDH releasing in OPCs in vitro.

The above findings recapitulated that the application of hepcidin reduced ferroptosis. Whether the ferroptosis occurred in the oligodendrocytes, the primary OPCs was firstly cultured. The immunostaining images illustrated that the cultured cells expressed NG2 and PDGFαR (Fig. 4A), demonstrating that the cultured cells were oligodendrocytes. Our previous study has represented that the iron concentration was about 30 μM/g in the epicenter of injured spinal cords [1], then 20 μM $FeCl_3$ was used to simulate the iron content in vitro experiments. The results revealed that the ROS level was prominently increased from 0.5 h to 48 h (Fig. 4B, C), while the application of hepcidin markedly decreased the content of ROS (Fig. 4B, C). At the same time, the cell viability was clearly decreased in group with the addition of 20 μM $FeCl_3$, while it was greatly reversed with the treatment of hepcidin in OPCs reflecting by absorbance value at 450 nm (Fig. 4D). Subsequently, the LDH releasing assays illustrated that the content of LDH was profoundly increased with the addition of 20 μM $FeCl_3$, whereas the administration of hepcidin partially overturned this effect (Fig. 4E). Collectively, these results demonstrated that iron evoked ferroptosis to decreased cell viability and increasing LDH activity, while the application of hepcidin markedly abolished this effect to minimize the ferroptosis level in OPCs.

3.5. Hepcidin alleviated ferroptosis through reducing the expression of DMT1 and TfR1 in OPCs in vitro.

The in vitro results supported that hepcidin reduced OPCs ferroptosis, and the mechanism was investigated based on the in vivo results that hepcidin mitigated ferroptosis through downregulating the expression of DMT1 and TfR1. Firstly, the results indicated that the gene expression of DMT1 and TfR1 was significantly upregulated with the addition of 20 μM $FeCl_3$ from 24 to 72 hours (Fig. 5A, B). Meanwhile, the administration of hepcidin clearly reduced the gene expression of DMT1 and TfR1 (Fig. 5C, D). Next, the immunoblot bands presented that the protein expression of DMT1 and TfR1 was obviously elevated with the treatment of 20 μM $FeCl_3$ from 24 to 72 hours (Fig. 6A-C). And, the application of hepcidin evidently downregulated the protein expression of DMT1 and TfR1 (Fig. 6D-F). Taken together, these results demonstrated that hepcidin inhibited OPCs ferroptosis by downregulating the expression of DMT1 and TfR1.

4. Discussion

SCI usually results in permanent or long-lasting neurological impairments, at least in part, ascribing to WMI [1, 2]. Oligodendrocytes are rich in unsaturated fatty acid [4] and susceptible to ferroptosis-induced damage [16]. Hepcidin holds the capacity of reducing iron content, thereafter mitigating ROS production and ferroptosis. However, the effect of hepcidin on ferroptosis in the epicenter of spinal cord remains elusive. Here, the results offer evidence that the administration of hepcidin reduces iron accumulation to promote oligodendrocytes survival and to decrease spinal cord atrophy, thereafter facilitating functional recovery. With the increased number of oligodendrocytes in the epicenter of spinal cord, the WMI is evidently decreased due to attenuating ferroptosis. Subsequently, the results uncover that the expression of DMT1 and TfR1 is expressed in $CC1^+$ cells. The expression of DMT1 and TfR1 is significantly increased, while the phenomenon is obviously neutralized with the administration of hepcidin in the epicenter of spinal cord after SCI. Afterward, the application of hepcidin downregulates enhanced ROS level, which is evidently increased with the treatment of 20 μM $FeCl_3$, thereafter increasing cell viability and reducing LDH activity through downregulating the expression of DMT1 and TfR1 to inhibit ferroptosis in OPCs. The present study provides evidence that the application of hepcidin expedites oligodendrocytes survival to alleviate WMI via minimizing the expression of DMT1 and TfR1.

Iron is an essential cofactor for the generation of cholesterol and phospholipids that are essential ingredients for efficient maturation of OPCs [30]. With the process of myelination, the expression of DMT1 and TfR1, two of iron uptake proteins, is elevated to promote iron deposition resulting in OPCs maturation [21, 31], which might be the reason why the expression of DMT1 and TfR1 remains higher level on day 56 post-SCI. Meanwhile, our previous study has indicated that SCI usually evokes iron accumulation in the epicenter of injured spinal cord [1], which positively induces the iron deposition in cytoplasm through the upregulation of DMT1 and TfR1 [32, 33]. Thereafter, the ROS level is significantly increased due to iron accumulation to trigger ferroptosis [1, 33], which is in consistence with the results that the ROS level is evidently elevated to evoke ferroptosis in oligodendrocytes with the administration of 20 μM $FeCl_3$ in present study. Thence, exploring approach to downregulate the expression of DMT1 and TfR1 is a feasible method to reduce oligodendrocytes ferroptosis, thereafter alleviating WMI after SCI.

Here, our results demonstrates that hepcidin is a suitable candidate to reduce ferroptosis through decreasing the expression of DMT1 and TfR1. Hepcidin is a secreted peptide hormone, and firstly isolated from blood and urine in human [34, 35]. Previous studies have reported hepcidin is dramatically downregulated in hippocampal lysates from mouse Alzheimer's disease (AD) brains along with the presence of iron overload [36, 37], suggesting that the administration of hepcidin is a suitable regimen for the reduction of iron concentration in CNS. And, SCI usually triggers iron accumulation not only in the epicenter of spinal cord [1, 17, 26, 38] but also in the motor cortex [20] both in animal SCI model and human. However, the application of hepcidin obviously decreases the iron content to downregulate ferroptosis in the epicenter of spinal cord following SCI. Meanwhile, another reason for the administration of hepcidin promoting functional recovery is that hepcidin holds the ability of inhibiting inflammatory process due to reducing IL-6 expression and secretion in astrocytes and microglia [39], indicating that

hepcidin could serve as a neuroinflammatory suppressor. Together, the application of hepcidin exerts neuroprotective effect, at least in part, due to reducing ferroptosis and neuroinflammation.

5. Conclusions

In conclusion, the present study provides direct evidence that the administration of hepcidin significantly downregulates iron overload and ferroptosis in the epicenter of spinal cord, thereafter facilitating oligodendrocytes survival to alleviating WMI following SCI in rats. With the reduction of WMI, the functional recovery is obviously improved post-SCI. This study enlarges the therapeutic scope of hepcidin on SCI, and even for other CNS diseases with the presence of ferroptosis.

Declarations

Funding

This work was supported by grants from the National Natural Science Foundation of China (approval no. 81471261) and Natural Science Foundation of Chongqing (approval no. cstc2018jcyjAX0080).

Compliance with Ethical Standards

Disclosure of potential conflicts of interest

The authors have no relevant financial or non-financial interests to disclose.

Research involving Animals

The animal experiment procedures were implemented according to the China’s animal welfare legislation for the protection of animals used for scientific purposes, and supervised by the Ethics Committee of the Southwest Hospital, Third Military Medical University (Army Medical University) for the use of laboratory animals (approval no. AMUWEC20210017).

Informed consent

Not applicable.

Consent to participate

Not applicable.

Consent for Publication

Not applicable.

Author contributions

Xingsen Xue and Guanjian He performed most of the experiments, with assistance from Linbo Yuan, Zhouyang Jiang, Long Wang, Jiantao Shi, Jiali Zhang, and Hong Su. Zhouyang Jiang and Long Wang analyzed the results and edited figures. Xingsen Xue, Linbo Yuan, and Jiantao Shi performed SCI model and statistical analysis. Guanjian He and Jiali Zhang performed cell culture and treatments. Xingsen Xue, Guangjian He, and Hong Su performed immunoblotting and immunostaining. Xingsen Xue wrote preliminary draft of the manuscript. Chuhua Fu designed experiments. Shengli Hu made the hypothesis and revised the manuscript. All authors approved final version of the manuscript.

Conflict of interest

The authors declare they have no conflict of interest.

Acknowledge

Not applicable.

Data Availability of data and materials

The data that support the findings of this study are available from the corresponding author upon reasonable request.

References

1. Ge H, Xue X, Xian J, Yuan L, Wang L, Zou Y, Zhong J, Jiang Z, Shi J, Chen T, Su H, Feng H, Hu S (2022) Ferrostatin-1 Alleviates White Matter Injury Via Decreasing Ferroptosis Following Spinal Cord Injury. Mol Neurobiol 59(1):161–176. doi:10.1007/s12035-021-02571-y
2. Krupa P, Svobodova B, Dubisova J, Kubinova S, Jendelova P, Machova Urdzikova L (2019) Nano-formulated curcumin (Lipodisq™) modulates the local inflammatory response, reduces glial scar and preserves the white matter after spinal cord injury in rats. Neuropharmacology 155:54–64. doi:10.1016/j.neuropharm.2019.05.018
3. Yuan J, Liu W, Zhu H, Chen Y, Zhang X, Li L, Chu W, Wen Z, Feng H, Lin J (2017) Curcumin inhibits glial scar formation by suppressing astrocyte-induced inflammation and fibrosis in vitro and in vivo. Brain Res 1655:90–103. doi:10.1016/j.brainres.2016.11.002
4. Xia Y, Zhao T, Li J, Li L, Hu R, Hu S, Feng H, Lin J (2008) Antisense vimentin cDNA combined with chondroitinase ABC reduces glial scar and cystic cavity formation following spinal cord injury in rats. Biochem Biophys Res Commun 377(2):562–566. doi:10.1016/j.bbrc.2008.10.024
5. Xia Y, Yan Y, Xia H, Zhao T, Chu W, Hu S, Feng H, Lin J (2015) Antisense vimentin cDNA combined with chondroitinase ABC promotes axon regeneration and functional recovery following spinal cord injury in rats. Neurosci Lett 590:74–79. doi:10.1016/j.neulet.2015.01.073
6. Hu R, Duan B, Wang D, Yu Y, Li W, Luo H, Lu P, Lin J, Zhu G, Wan Q, Feng H (2011) Role of acid-sensing ion channel 1a in the secondary damage of traumatic spinal cord injury. Ann Surg

254(2):353–362. doi:10.1097/SLA.0b013e31822645b4

7. Hu R, Sun H, Zhang Q, Chen J, Wu N, Meng H, Cui G, Hu S, Li F, Lin J, Wan Q, Feng H (2012) G-protein coupled estrogen receptor 1 mediated estrogenic neuroprotection against spinal cord injury. Crit Care Med 40(12):3230–3237. doi:10.1097/CCM.0b013e3182657560
8. Chen J, Hu R, Ge H, Duanmu W, Li Y, Xue X, Hu S, Feng H (2015) G-protein-coupled receptor 30-mediated antiapoptotic effect of estrogen on spinal motor neurons following injury and its underlying mechanisms. Mol Med Rep 12(2):1733–1740. doi:10.3892/mmr.2015.3601
9. Li L, Xiong ZY, Qian ZM, Zhao TZ, Feng H, Hu S, Hu R, Ke Y, Lin J (2014) Complement C5a is detrimental to histological and functional locomotor recovery after spinal cord injury in mice. Neurobiol Dis 66:74–82. doi:10.1016/j.nbd.2014.02.008
10. Chu W, Yuan J, Huang L, Xiang X, Zhu H, Chen F, Chen Y, Lin J, Feng H (2015) Valproic Acid Arrests Proliferation but Promotes Neuronal Differentiation of Adult Spinal NSPCs from SCI Rats. Neurochem Res 40(7):1472–1486. doi:10.1007/s11064-015-1618-x
11. Chen F, Wang H, Xiang X, Yuan J, Chu W, Xue X, Zhu H, Ge H, Zou M, Feng H, Lin J (2014) Curcumin increased the differentiation rate of neurons in neural stem cells via wnt signaling in vitro study. J Surg Res 192(2):298–304. doi:10.1016/j.jss.2014.06.026
12. Hu SL, Luo HS, Li JT, Xia YZ, Li L, Zhang LJ, Meng H, Cui GY, Chen Z, Wu N, Lin JK, Zhu G, Feng H (2010) Functional recovery in acute traumatic spinal cord injury after transplantation of human umbilical cord mesenchymal stem cells. Crit Care Med 38(11):2181–2189. doi:10.1097/CCM.0b013e3181f17c0e
13. Mekhail M, Almazan G, Tabrizian M (2012) Oligodendrocyte-protection and remyelination post-spinal cord injuries: a review. Prog Neurobiol 96(3):322–339. doi:10.1016/j.pneurobio.2012.01.008
14. Fehlings MG, Tator CH (1995) The relationships among the severity of spinal cord injury, residual neurological function, axon counts, and counts of retrogradely labeled neurons after experimental spinal cord injury. Exp Neurol 132(2):220–228. doi:10.1016/0014-4886(95)90027-6
15. Kakulas BA (1999) A review of the neuropathology of human spinal cord injury with emphasis on special features. J Spinal Cord Med 22(2):119–124. doi:10.1080/10790268.1999.11719557
16. Jhelum P, Santos-Nogueira E, Teo W, Haumont A, Lenoël I, Stys PK, David S (2020) Ferroptosis Mediates Cuprizone-Induced Loss of Oligodendrocytes and Demyelination. J neuroscience: official J Soc Neurosci 40(48):9327–9341. doi:10.1523/jneurosci.1749-20.2020
17. Chen Y, Liu S, Li J, Li Z, Quan J, Liu X, Tang Y, Liu B (2020) The Latest View on the Mechanism of Ferroptosis and Its Research Progress in Spinal Cord Injury. Oxidative medicine and cellular longevity 2020:6375938. doi:10.1155/2020/6375938
18. Li Q, Weiland A, Chen X, Lan X, Han X, Durham F, Liu X, Wan J, Ziai WC, Hanley DF, Wang J (2018) Ultrastructural Characteristics of Neuronal Death and White Matter Injury in Mouse Brain Tissues After Intracerebral Hemorrhage: Coexistence of Ferroptosis, Autophagy, and Necrosis. Front Neurol 9:581. doi:10.3389/fneur.2018.00581

19. Yao X, Zhang Y, Hao J, Duan HQ, Zhao CX, Sun C, Li B, Fan BY, Wang X, Li WX, Fu XH, Hu Y, Liu C, Kong XH, Feng SQ (2019) Deferoxamine promotes recovery of traumatic spinal cord injury by inhibiting ferroptosis. Neural regeneration research 14(3):532–541. doi:10.4103/1673-5374.245480
20. Feng Z, Min L, Chen H, Deng W, Tan M, Liu H, Hou J (2021) Iron overload in the motor cortex induces neuronal ferroptosis following spinal cord injury. Redox Biol 43:101984. doi:10.1016/j.redox.2021.101984
21. Qian ZM, Ke Y (2020) Hepcidin and its therapeutic potential in neurodegenerative disorders. Med Res Rev 40(2):633–653. doi:10.1002/med.21631
22. Ganz T (2013) Systemic iron homeostasis. Physiol Rev 93(4):1721–1741. doi:10.1152/physrev.00008.2013
23. Ge XH, Wang Q, Qian ZM, Zhu L, Du F, Yung WH, Yang L, Ke Y (2009) The iron regulatory hormone hepcidin reduces ferroportin 1 content and iron release in H9C2 cardiomyocytes. J Nutr Biochem 20(11):860–865. doi:10.1016/j.jnutbio.2008.07.014
24. Du F, Qian ZM, Luo Q, Yung WH, Ke Y (2015) Hepcidin Suppresses Brain Iron Accumulation by Downregulating Iron Transport Proteins in Iron-Overloaded Rats. Mol Neurobiol 52(1):101–114. doi:10.1007/s12035-014-8847-x
25. Du F, Qian C, Qian ZM, Wu XM, Xie H, Yung WH, Ke Y (2011) Hepcidin directly inhibits transferrin receptor 1 expression in astrocytes via a cyclic AMP-protein kinase A pathway. Glia 59(6):936–945. doi:10.1002/glia.21166
26. Shi J, Tang R, Zhou Y, Xian J, Zuo C, Wang L, Wang J, Feng H, Hu S (2020) Attenuation of White Matter Damage Following Deferoxamine Treatment in Rats After Spinal Cord Injury. World Neurosurg 137:e9–e17. doi:10.1016/j.wneu.2019.08.246
27. Basso DM, Beattie MS, Bresnahan JC (1995) A sensitive and reliable locomotor rating scale for open field testing in rats. J Neurotrauma 12(1):1–21. doi:10.1089/neu.1995.12.1
28. Hu SL, Lu PG, Zhang LJ, Li F, Chen Z, Wu N, Meng H, Lin JK, Feng H (2012) In vivo magnetic resonance imaging tracking of SPIO-labeled human umbilical cord mesenchymal stem cells. J Cell Biochem 113(3):1005–1012. doi:10.1002/jcb.23432
29. Jiang X, Zhang J, Kou B, Zhang C, Zhong J, Fang X, Huang X, Zhang X, Xie F, Hu Q, Ge H, Yu A (2020) Ambroxol Improves Neuronal Survival and Reduces White Matter Damage through Suppressing Endoplasmic Reticulum Stress in Microglia after Intracerebral Hemorrhage. Biomed Res Int 2020:8131286. doi:10.1155/2020/8131286
30. Cheli VT, Correale J, Paez PM, Pasquini JM (2020) Iron Metabolism in Oligodendrocytes and Astrocytes, Implications for Myelination and Remyelination. ASN neuro 12:1759091420962681. doi:10.1177/1759091420962681
31. Cheli VT, Santiago González DA, Marziali LN, Zamora NN, Guitart ME, Spreuer V, Pasquini JM, Paez PM (2018) The Divalent Metal Transporter 1 (DMT1) Is Required for Iron Uptake and Normal Development of Oligodendrocyte Progenitor Cells. J neuroscience: official J Soc Neurosci 38(43):9142–9159. doi:10.1523/jneurosci.1447-18.2018

32. Zhang L, Wang Z, Song C, Liu H, Li Y, Li J, Yu Y, Wang G, Cui W (2021) Spinal NR2B phosphorylation at Tyr1472 regulates IRE(-)DMT1-mediated iron accumulation and spine morphogenesis via kalirin-7 in tibial fracture-associated postoperative pain after orthopedic surgery in female mice. Reg Anesth Pain Med 46(4):363–373. doi:10.1136/rapm-2020-101883
33. Park E, Chung SW (2019) ROS-mediated autophagy increases intracellular iron levels and ferroptosis by ferritin and transferrin receptor regulation. Cell Death Dis 10(11):822. doi:10.1038/s41419-019-2064-5
34. Krause A, Neitz S, Mägert HJ, Schulz A, Forssmann WG, Schulz-Knappe P, Adermann K (2000) LEAP-1, a novel highly disulfide-bonded human peptide, exhibits antimicrobial activity. FEBS Lett 480(2–3):147–150. doi:10.1016/s0014-5793(00)01920-7
35. Park CH, Valore EV, Waring AJ, Ganz T (2001) Hepcidin, a urinary antimicrobial peptide synthesized in the liver. J Biol Chem 276(11):7806–7810. doi:10.1074/jbc.M008922200
36. Raha AA, Vaishnav RA, Friedland RP, Bomford A, Raha-Chowdhury R (2013) The systemic iron-regulatory proteins hepcidin and ferroportin are reduced in the brain in Alzheimer's disease. Acta Neuropathol Commun 1:55. doi:10.1186/2051-5960-1-55
37. Derry PJ, Hegde ML, Jackson GR, Kayed R, Tour JM, Tsai AL, Kent TA (2020) Revisiting the intersection of amyloid, pathologically modified tau and iron in Alzheimer's disease from a ferroptosis perspective. Prog Neurobiol 184:101716. doi:10.1016/j.pneurobio.2019.101716
38. Blomster LV, Cowin GJ, Kurniawan ND, Ruitenberg MJ (2013) Detection of endogenous iron deposits in the injured mouse spinal cord through high-resolution ex vivo and in vivo MRI. NMR Biomed 26(2):141–150. doi:10.1002/nbm.2829
39. Urrutia PJ, Hirsch EC, González-Billault C, Núñez MT (2017) Hepcidin attenuates amyloid beta-induced inflammatory and pro-oxidant responses in astrocytes and microglia. J Neurochem 142(1):140–152. doi:10.1111/jnc.14005

Figures

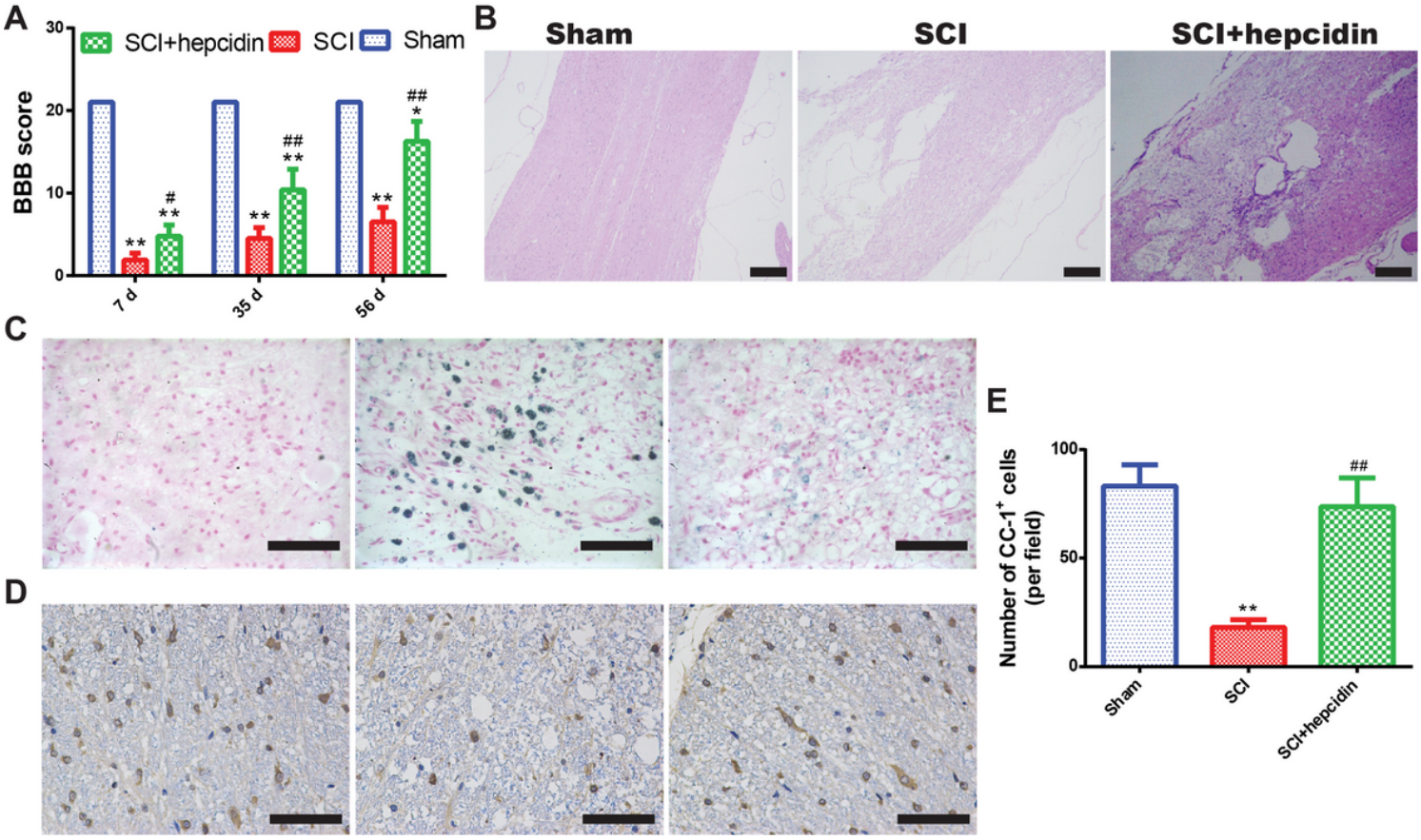

Figure 1

Hepcidin facilitated functional recovery through reducing iron deposition and facilitating the survival of oligodendrocytes after SCI.

(A) Histogram demonstrating the Basso, Beattie and Bresnahan (BBB) score in each group on days 7, 35 and 56 following SCI. N=7; $^{*}p<0.05$, $^{**}p<0.01$ *vs* Sham group; $^{\#}p<0.05$, $^{\#\#}p<0.01$ *vs* SCI group; two-way ANOVA, followed by Tukey's post hoc test. **(B)** HE staining showing the status of spinal cord on day 7 following SCI. Scale bars: 200 μm. N=4 per group. **(C)** Perl's blue staining images depicting the iron accumulation in the epicenter of injured spinal cord on day 7 in different groups. Scale bar: 50 μm. N=4 per group. **(D)** Immunohistochemistry images indicating the $CC1^{+}$ cells in the epicenter of injured spinal cord in each group on day 7. Scale bar: 50 μm. **(E)** Bar chart illustrating the number of $CC1^{+}$ cells from (D). N=4; $^{**}p<0.01$ *vs* Sham group; $^{\#\#}p<0.01$ *vs* SCI group; one-way ANOVA, followed by Tukey's post hoc test.

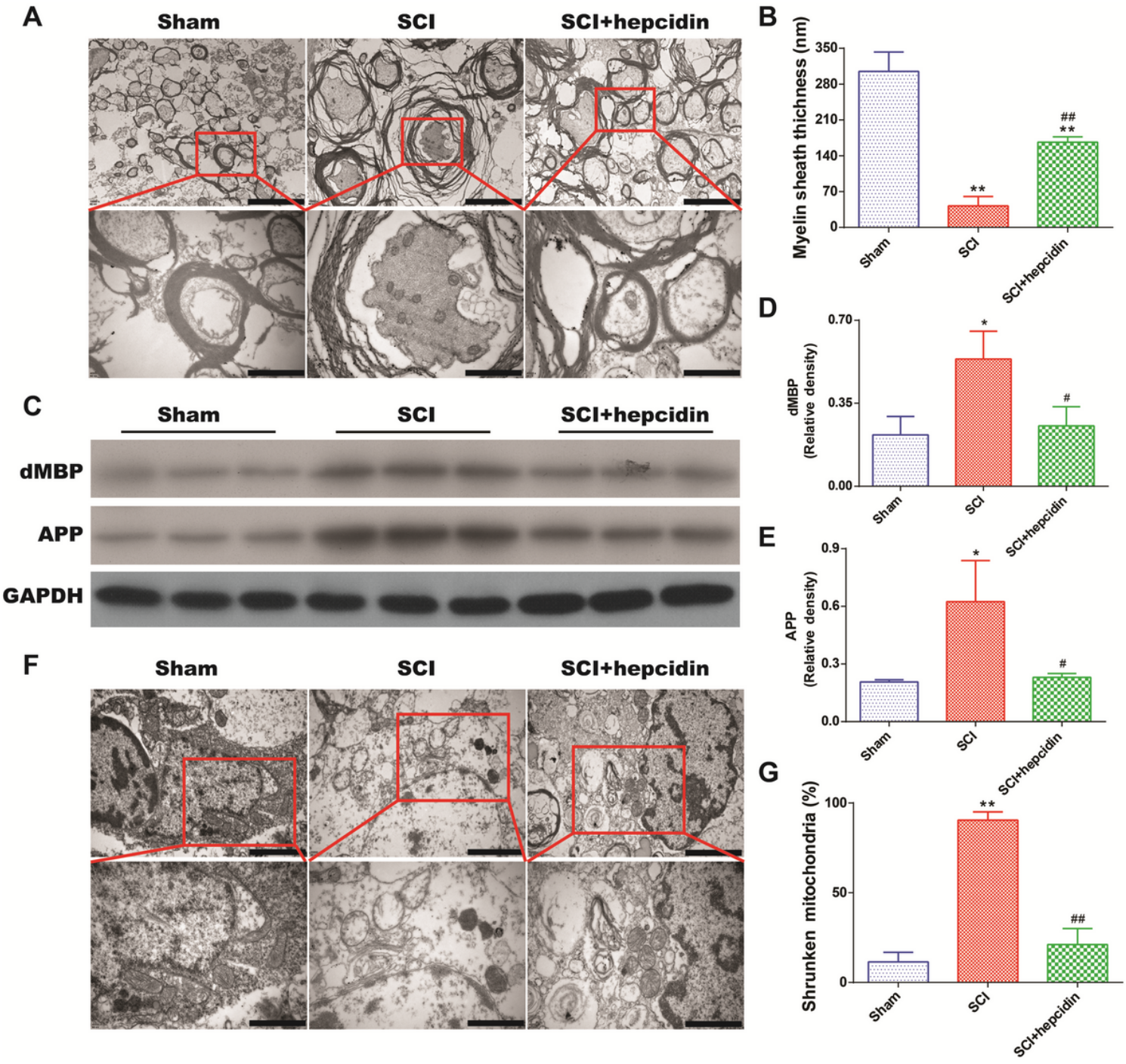

Figure 2

Hepcidin reduced white matter injury (WMI) by alleviating ferroptosis post-SCI.

(A) Transmission electron microscopy (TEM) images showcasing the myelin sheath thickness in each group on day 7 post-SCI. Scale bars: 5 μm; 1 μm for enlarged inserts. **(B)** Bar graph showing the myelin sheath thickness from (A). N=4; $^{**}p<0.01$ *vs* Sham group; $^{\#\#}p<0.01$ *vs* SCI group; one-way ANOVA, followed by Tukey's post hoc test. **(C)** Immunoblot bands representing the expression levels of dMBP and APP in various groups. GAPDH was loaded as an internal control. **(D, E)** Semi-quantification of the expression of dMBP (D) and APP (E) from (C). N=3; $^{*}p<0.05$ *vs* Sham group; $^{\#}p<0.05$ *vs* SCI group; one-

way ANOVA, followed by Tukey's post hoc test. **(F)** TEM images showing the morphological changes of mitochondria in each group on day 7 post-SCI. Scale bars: 5 μm; 1 μm for enlarged inserts. **(G)** Histogram summarizing the percentage of shrunken mitochondria from (F). N=4; $^{**}p<0.01$ *vs* Sham group; $^{\#\#}p<0.01$ *vs* SCI group; one-way ANOVA, followed by Tukey's post hoc test.

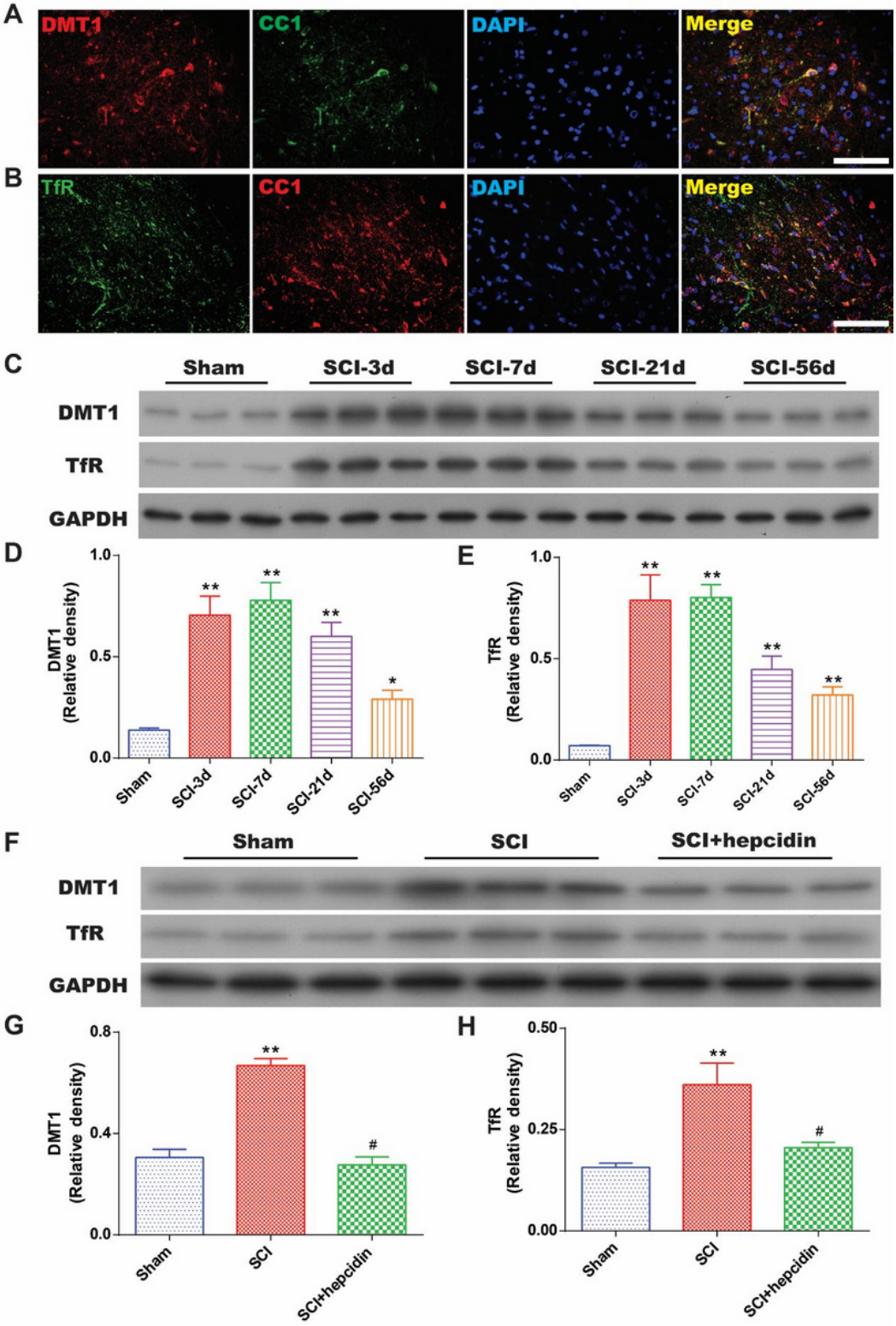

Figure 3

Hepcidin mitigated ferroptosis via decreasing the expression of DMT1 and TfR after SCI.

(A) Immunostaining images depicting the co-labelling of DMT1 (red) and CC1 (green) in each group on day 7 post-SCI. Scale bar: 50 μm. **(B)** Immunostaining images depicting the co-localization of TfR (green) and CC1 (red) in each group on day 7 after SCI. Scale bar: 50 μm. **(C)** Immunoblot bands depicting the expression levels of DMT1 and TfR on days 3, 7, 21 and 56 post-SCI. GAPDH was loaded as an internal control. **(D, E)** Semi-quantification of the expression of DMT1 (D) and TfR (E) from (C). N=3; $^{*}p<0.05$, $^{**}p<0.01$ *vs* Sham group; one-way ANOVA, followed by Tukey's post hoc test. **(F)** Immunoblot bands showing the expression levels of DMT1 and TfR in different groups post-SCI. GAPDH was loaded as an internal control. **(G, H)** Semi-quantification of the expression of DMT1 (D) and TfR (E) from (F). N=3; $^{**}p<0.01$ *vs* Sham group; $^{\#}p<0.05$ *vs* SCI group; one-way ANOVA, followed by Tukey's post hoc test.

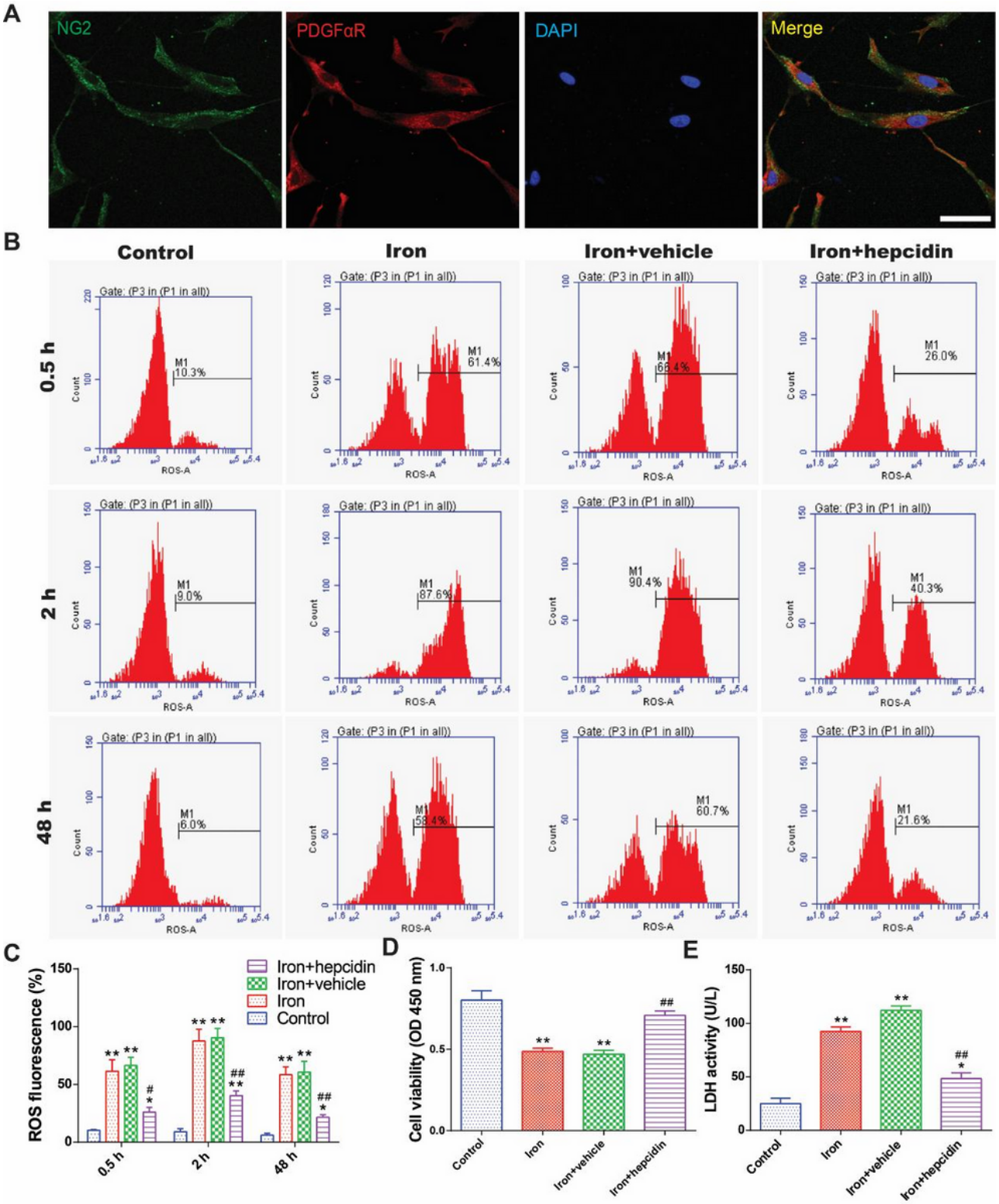

Figure 4

Hepcidin reduced ROS accumulation to increase cell viability and reduce LDH releasing in vitro.

(A) Immunostaining images demonstrating the expression of NG2 (green) and PDGFαR (red) in primary OPCs. Scale bars: 20 μm. **(B)** Representational images demonstrating the ROS accumulation using flow cytometry. **(C)** Histogram summarizing the percentage of ROS fluorescence from (A). N=3; $^{*}p<0.05$,

$^{**}p<0.01$ *vs* Control group; $^{\#}p<0.05$, $^{\#\#}p<0.01$ *vs* Iron group; two-way ANOVA, followed by Tukey's post hoc test. **(D)** Bar graph illustrating the absorbance value at 450 nm in each group. N=6; $^{**}p<0.01$ *vs* Control group; $^{\#\#}p<0.01$ *vs* Iron group and Iron+hepcidin group; one-way ANOVA, followed by Tukey's post hoc test. **(E)** LDH releasing assays in each group. N=6; $^{**}p<0.01$, $^{*}p<0.05$ *vs* Control group; $^{\#\#}p<0.01$ *vs* Iron group and Iron+vehicle group; one-way ANOVA, followed by Tukey's post hoc test.

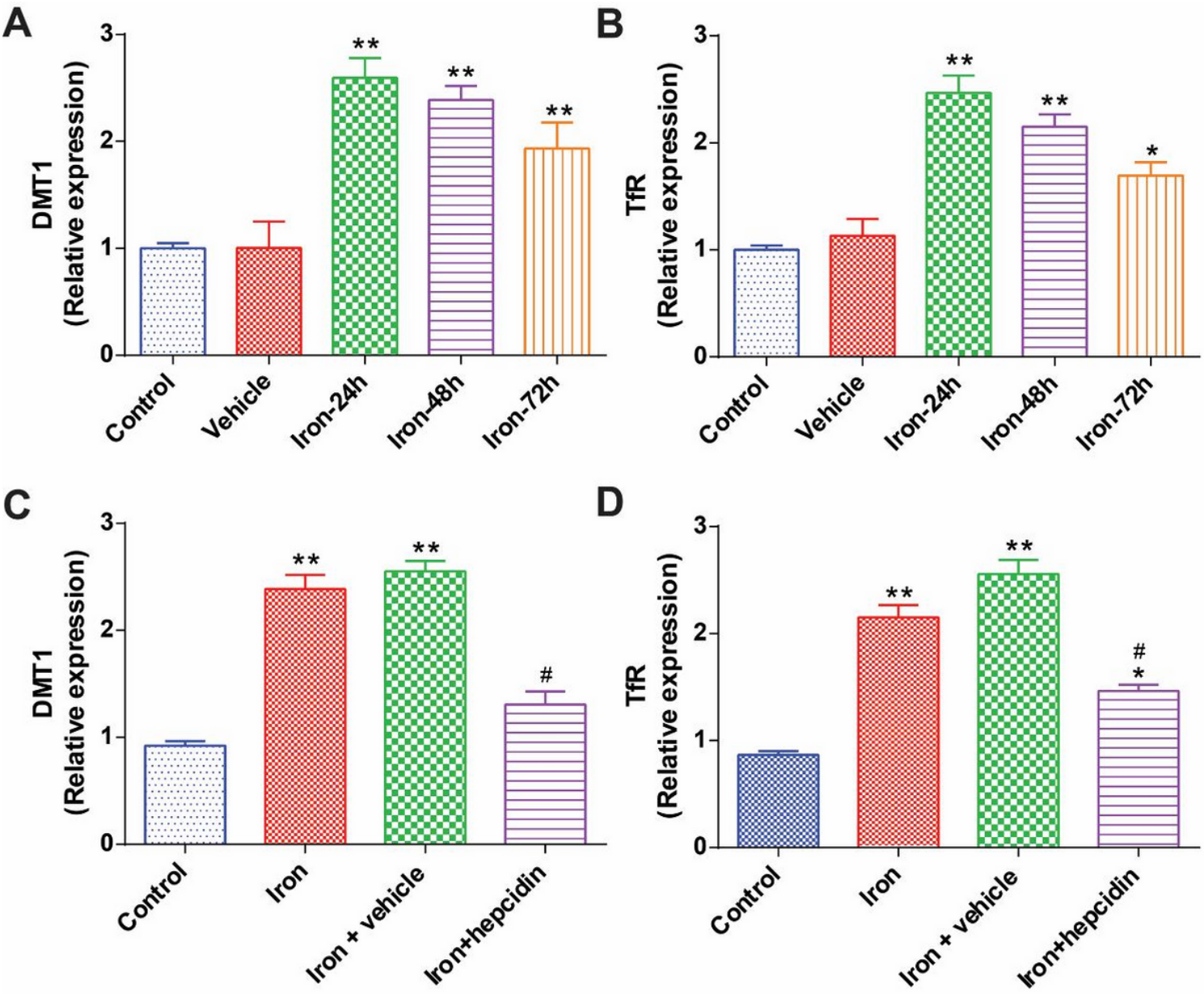

Figure 5

Hepcidin decreased the gene expression of DMT1 and TfR to mitigate OPCs ferroptosis resulting from iron overload.

(A, B) Quantification of the gene expression of DMT1 (A) and TfR (B) determined by RT-qPCR in each group at different time points. N=4; $^{**}p<0.01$, $^{*}p<0.05$ *vs* Control group and Vehicle group. **(C, D)** Quantification of the gene expression of DMT1 (C) and TfR (D) assessed using RT-qPCR in each group.

N=4; $^{**}p<0.01$, $^{*}p<0.05$ *vs* Control group group; $^{\#}p<0.05$ *vs* Iron group and Iron+vehicle group; one-way ANOVA, followed by Tukey's post hoc test.

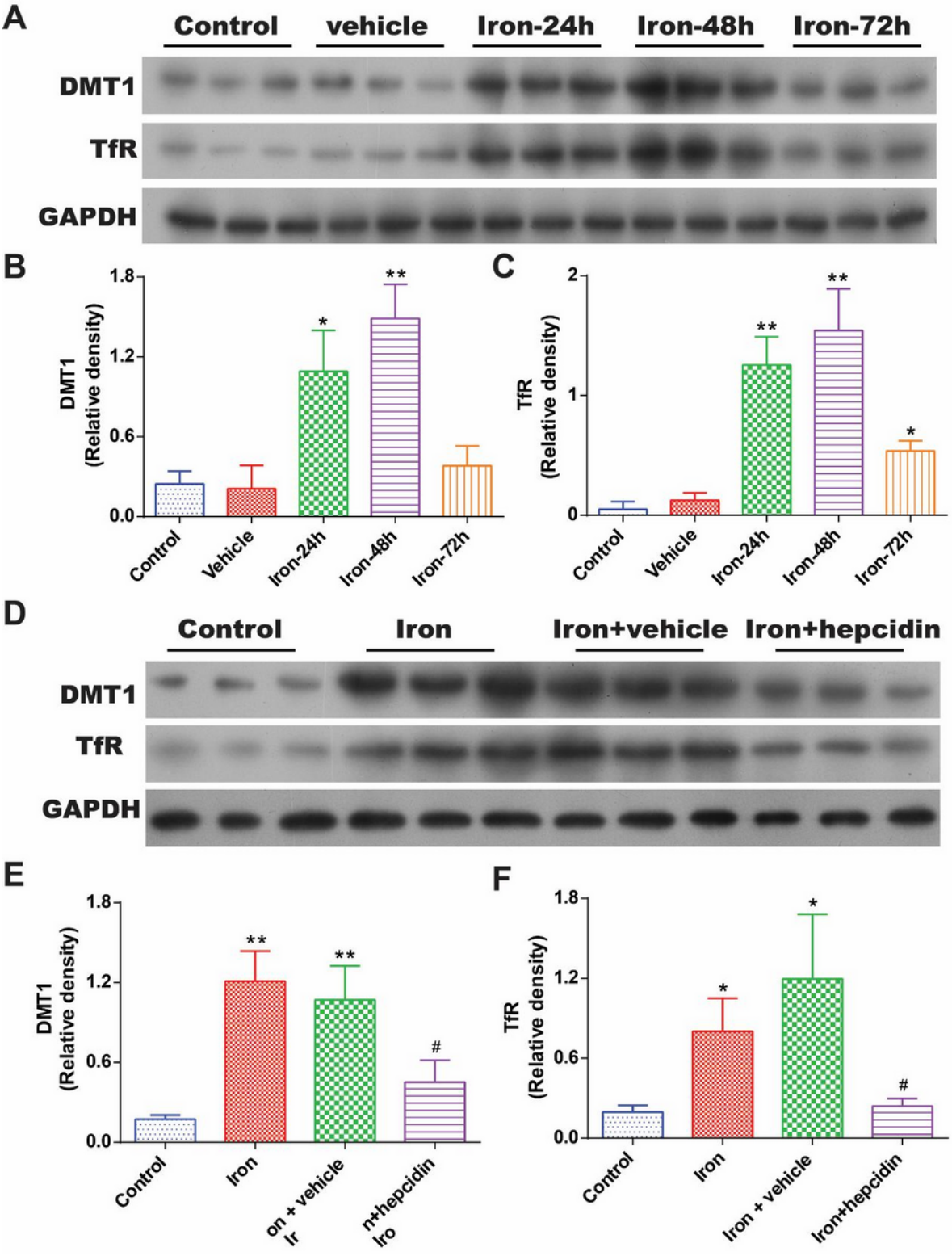

Figure 6

Hepcidin reduced the expression of DMT1 and TfR to mitigate OPCs ferroptosis deriving from iron accumulation.

(A) Immunoblot bands representing the expression levels of DMT1 and TfR in each group at different time points. GAPDH was loaded as an internal control. **(B, C)** Semi-quantification of the expression of DMT1 (B) and TfR (C) from (A). N=4; $^{**}p<0.01$, $^{*}p<0.05$ *vs* Control group and Vehicle group; one-way ANOVA, followed by Tukey's post hoc test. **(D)** Immunoblot bands representing the expression levels of DMT1 and TfR in each group. GAPDH was loaded as an internal control. **(E, F)** Semi-quantification of the expression of DMT1 (E) and TfR (F) from (D). N=4; $^{**}p<0.01$, $^{*}p<0.05$ *vs* Control group; $^{\#}p<0.05$ *vs* Iron group and Iron+vehicle group; one-way ANOVA, followed by Tukey's post hoc test.